International Journal of Medical, Medicine and Health Sciences
ISSN: 2517-9969
Vol:7, No:6, 2013

# Automatic Microaneurysm Quantification for Diabetic Retinopathy Screening

A. Sopharak, B. Uyyanonvara, and S. Barman

***Abstract*—**Microaneurysm is a key indicator of diabetic retinopathy that can potentially cause damage to retina. Early detection and automatic quantification are the keys to prevent further damage. In this paper, which focuses on automatic microaneurysm detection in images acquired through non-dilated pupils, we present a series of experiments on feature selection and automatic microaneurysm pixel classification. We found that the best feature set is a combination of 10 features: the pixel's intensity of shade corrected image, the pixel hue, the standard deviation of shade corrected image, DoG4, the area of the candidate MA, the perimeter of the candidate MA, the eccentricity of the candidate MA, the circularity of the candidate MA, the mean intensity of the candidate MA on shade corrected image and the ratio of the major axis length and minor length of the candidate MA. The overall sensitivity, specificity, precision, and accuracy are 84.82%, 99.99%, 89.01%, and 99.99%, respectively.

***Keywords*—**Diabetic retinopathy, microaneurysm, naive Bayes classifier

## I. Introduction

DIABETIC retinopathy (DR) is a severe eye disease and a major cause of blindness [1]. Microaneurysm appeared at the earliest clinically localized characteristic of DR, their detection would help to early treatment and prevent the blindness. Diabetes patients need to have eye screening each year in order to prevent the blindness. However, manual examination by ophthalmologists takes time and the number of ophthalmologists is not sufficient to cope with all patients.

In this paper we concentrate on MA detection as the earliest clinically localized characteristic of DR [2]. Retinal MAs are focal dilatations of retinal capillaries. They are discrete, localized saccular distensions of the weakened capillary walls and appear as small round dark red dots on the retinal surface. The diameter of a MA lies between 10 and 100 μm, but it always smaller then a diameter $\lambda < 125$ μm [2], [3].

Most of the previous researches is based on imagery acquired after dilating the pupils, e.g. with Tropicamide eye drops, in which MA and other retinal features are clearly visible.

A few attempts are based on morphological technique. T. Spencer et al. [3], M.J. Cree et al. [4] and A. Frame et al. [5] employ a mathematical morphology technique to segment MA within fluorescein angiograms. T. Walter et al. [6] propose a method based on diameter closing and kernel density estimation for automatic classification.

Some are based on region growing. C. Sinthanayothin et al. [7] propose an automated system of detection of diabetic retinopathy using recursive region growing segmentation (RRGS). D. Usher et al. [8] employ a combination of RRGS and adaptive intensity thresholding to detect candidate lesion regions and a neural network is used for classification.

Clustering has also been proposed. B. Dupas et al. [9] use a diameter-closing to segment MA candidate regions and k-nearest neighbours (kNN) to classify MA. M. Niemeijer et al. [10] combine prior works by T. Spencer et al. [3] and A. Frame et al. [5] with a detection system based on pixel classification and new features are proposed. A kNN classifier was used in the final step. Gardner et al. [11] use a back propagation neural network on sub-images (20x20 or 30x30 pixel windows). B. Zhang et al. [12] use multi-scale correlation coefficients (MSCF). They detect coarse MA candidate using MSCF and fine MA using features classification.

In previous work, we have proposed MA detection using mathematical morphology [13]. Here we take a machine learning approach to the problem of MA classification. Our method performs MA feature selection and classification using naive Bayes classifier. The optimal feature selection is proposed.

The proposed system includes noise removal, contrast enhancement and shade correction. Vessels, exudates and optic disc are also detected and removed. The candidate MAs are detected by using a set of optimally adjusted mathematical morphology. The MA features are extracted, and then classified those features using a model built from a training set. The final classifier is a substantial improvement on previous work.

## II. Method

The 45 digital retinal images taken from patients with non-dilated pupils were obtained from a KOWA-7 non-mydriatic retinal camera with a 45° field of view. The image size is 752

Sopharak. A. is with Faculty of Science and Arts, Burapha University Chanthaburi Campus, 57 Moo.1 Kamong, Thamai, Chanthaburi, THAILAND 22170 (phone: +66-39-310000; fax: +66-39-310128; e-mail: akara@buu.ac.th).

Uyyanonvara. B. is with Sirindhorn International Institute of Technology, Thammasart University, 131 Moo. 5 Tiwanont Road, Bangkadi, Muang, Pathumthani, THAILAND (e-mail: bunyarit@siit.tu.ac.th).

Barman. S. is with Kingston University, Penrhyn Road, Kingston Upon Thames, Surrey, KT1 2EE, United Kingdom (e-mail: S.Barman@kingston.ac.uk).

x 500 pixels with 24 bits per pixel.

*A. Preprocessing*

The green plane ($f_g$) of the original image in RGB plane is used as red lesions such as MA and blood vessels have the highest contrast with the background in this color plane. A median filtering operation is applied on $f_g$ to attenuate the noise before a Contrast Limited Adaptive Histogram Equalization was applied for contrast enhancement. A shade correction algorithm is applied to the green band in order to remove slow background variation due to non-uniform illumination. Original RGB and shade corrected images are shown in Fig. 1.

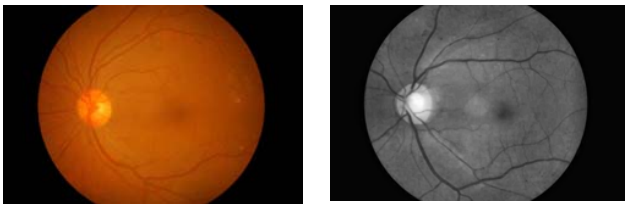

(a) (b)

Fig. 1 Retinal image (a) original RGB image (b) Shade corrected image

*B. Bright Lesions Detection*

We have to remove bright lesions such as exudates prior to the process because when they lie close together, small islands are formed between them and they can be wrongly detected as MAs. The morphological reconstruction method is used for exudate detection. The optic disc is also detected in order to avoid the false detection. The entropy and their compactness are computed [14].

*C. Vessels Detection*

Vessels are another element in the image that needs to be removed prior the MA detection since MA and vessels both appear in a reddish color and MAs cannot occur on vessels. Candidate vessels are detected by the difference between the image after closing operator and the filled-in small black dot image. The objects on the difference image which have size smaller than 10 pixels (in our image set of size 752 x 500 pixels, the size of a MA is about 10 pixels.) are then removed.

*D. MA Candidate Detection*

The extended-minima transform is applied to the shade corrected image ($f_{sc}$) image. It is the regional minima of h-minima transform. The output image $f_E$ is a binary image with the white pixels represent the regional minima in the original image. The extended minima transform on the $f_{sc}$ image with threshold value $\alpha_2$ ($\alpha_2 = 0.05$ is used) is shown in (1).

$$f_E = EM(f_{sc}, \alpha_2) \quad (1)$$

where $f_E$ is the output image.

The previous detected exudates, vessels and optic disc were removed from the resulting image. The result is shown in Fig. 2 (b).

(a) (b)

Fig. 2 Vessel and extended-minima transform image (a) vessel detected (b) extended-minima transform image

$$f_{VE\_removed} = f_E - f_{vesselT} - f_{ex} - f_{od} \quad (2)$$

where $f_{ex}$ is the exudate detected image and $f_{od}$ is the optic disc detected image.

*E. Feature Extraction*

A total feature set contains 18 features are proposed to distinguish MA pixels from non-MA pixels. All 18 features are z-scale (transform to a mean of 0 and a standard deviation of 1) using the statistics of each feature over the training set.

The list of 18 features is shown in Table I. Example of input images is shown in Fig. 3

TABLE I
MA EXTRACTED FEATURES

| No. | Description |
|---|---|
| 1 | *The pixel's intensity value of shade corrected image ($I_{sc}$)* |
| 2 | *The pixel's intensity value of green band image after preprocessing ($I_g$)* |
| 3 | *The pixel's hue* |
| 4 | *The standard deviation of shade corrected image.* A window size of 15x15 is used. |
| 5 | *The standard deviation of green band image after preprocessing.* A window size of 15x15 is used. |
| 6-11 | *Six Difference of Gaussian (DoG) filter responses. The DoG filter subtracts one blurred version of an original image from another blurred version of the image [16]. We convolve with seven different Gaussian kernels with standard deviations of 0.5, 1, 2, 4, 8, 16, and 32. We use DoG1, DoG2, DoG3, DoG4, DoG5 and DoG6 to refer to the features obtained by subtracting the image at scale $\sigma = 0.5$ from scale $\sigma = 1$, scale $\sigma = 1$ from $\sigma = 2$, scale $\sigma = 2$ from $\sigma = 4$, scale $\sigma = 4$ from $\sigma = 8$, scale $\sigma = 8$ from $\sigma = 16$, and scale $\sigma = 16$ from $\sigma = 32$, respectively* |
| 12 | *The area of the candidate MA* |
| 13 | *The perimeter of the candidate MA* |
| 14 | *The eccentricity of the candidate MA* |
| 15 | *The circularity of the candidate MA* |
| 16 | *The mean intensity of the candidate MA on shade corrected image* |
| 17 | *The mean intensity of the candidate MA on green band image* |
| 18 | *The ratio of the major axis length and minor length of the candidate MA* |

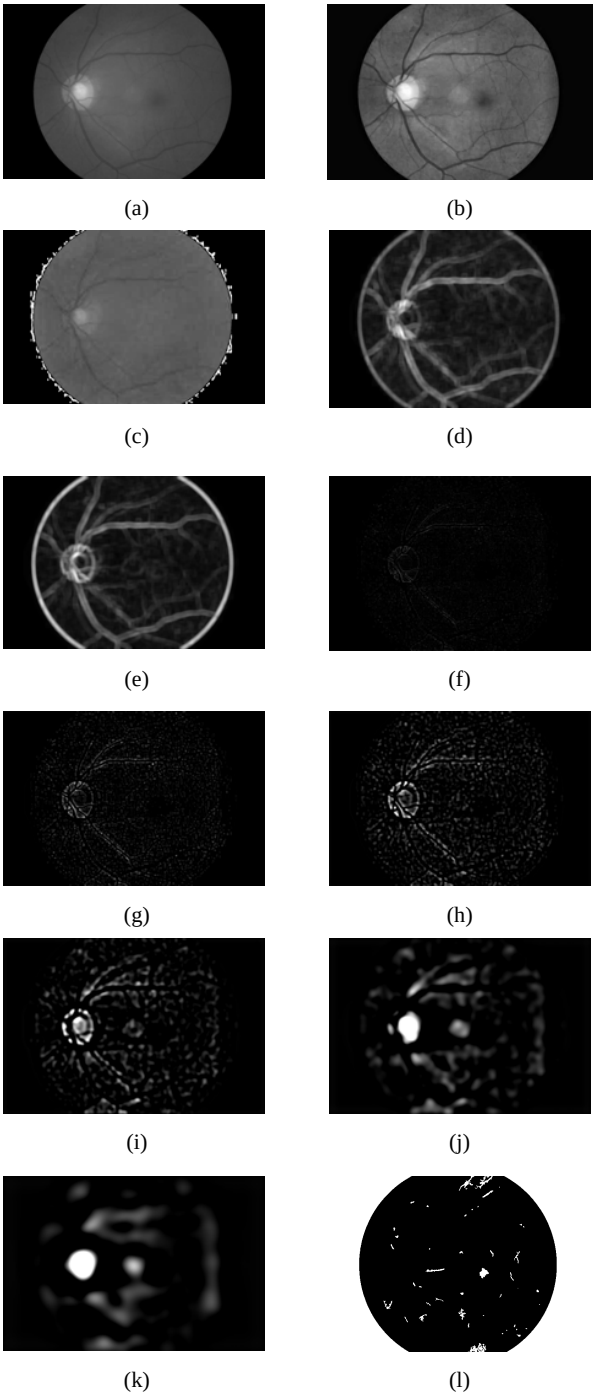


Fig. 3 Input features. (a) Intensity of green band image (b) Intensity of shade corrected image. (c) Hue (d) Standard deviation of green band image (e) Standard deviation of shade corrected image (f) DoG1 (g) DoG2 (h) DoG3 (i) DoG4 (j) DoG5 (k) DoG6 (l) MA candidate

*F. Features Selection and Classification Using Naive Bayes Classifier*

The naive Bayes classifier [15] - [17] uses the principle of Bayesian maximum a posteriori (MAP) classification: measure a finite set of features $\mathbf{x} = (x_1,\ldots, x_n)$ then select the class

$$\hat{y} = \arg\max_y P(y|\mathbf{x})$$

where

$$P(y|\mathbf{x}) \propto P(\mathbf{x}|y)P(y) \quad (3)$$

$P(\mathbf{x}|y)$ is the likelihood of feature vector $\mathbf{x}$ given class $y$, and $P(y)$ is the priori probability of class $y$. Naive Bayes assumes that the features are conditionally independent given the class:

$$P(\mathbf{x}|y) = \prod_i P(x_i|y)$$

We estimate the parameters $P(x_i|y)$ and $P(y)$ from training data.

After z-scaling, all of our features $x_i$ are continuous, but the simple version of naive Bayes just described requires discrete features, so we perform unsupervised proportional $k$-interval discretization as implemented in Weka [18]. The technique uses equal-frequency binning, where the number of bins is the square root of the number of values.

We first estimate the model of Equation 3 from a training set using all features then evaluate the resulting classifier's performance on a separate test set. Then we iteratively delete features until the average of the precision (PR) stops improving. On each step, for each feature, we delete that feature from the model, train a new classifier, and evaluate its performance on the test set. The PR of the best such classifier is compared to the PR of the classifier without deleted features. If PR improves, we permanently delete that feature then repeat the process. Finally, the best feature set and classifier are retained.

*G.Performance Measurement*

We evaluate performance on the test set quantitatively by comparing the classifier's result to ground truth. To obtain ground truth for each image, we used image processing software to hand label candidate MA regions, then we asked an ophthalmologist to verify or reject each candidate region. We split the 45-image data set into a training set containing 30 images and a test set containing 15 images. To evaluate classifier performance, we use sensitivity, specificity, PR and accuracy. Sensitivity is the percentage of the actual exudate pixels that are detected; specificity is the percentage of non-exudate pixels that are correctly classified as non-exudate pixels. PR is the percentage of detected pixels that are actually exudate. Accuracy is the overall per-pixel success rate of the classifier.

## III. Results

As a first experiment, we fit the naive Bayes to the training set using all 18 features. The resulting classifier had overall per-pixel sensitivity, specificity, PR and accuracy of 85.68%, 99.99%, 83.34%, 99.99% and 96.55%, respectively. On the next step, we backwardly removed features from the classifier

one at a time and compared each resulting PR value to the previous feature set's performance. We obtained the best PR value (81.78%) by deleting intensity of green band, presumably due to its redundancy with the shade corrected image intensity feature. We continued this process until the PR stopped improving. We obtained the final best-performing classifier by deleting intensity of green band image, standard deviation of green band image, DoG6, DoG5, DoG2, DoG1, mean intensity of the candidate MA on green band image and DoG3. Finally, the best-performing classifier contained ten features: the pixel's intensity of shade corrected image, the pixel hue, the standard deviation of shade corrected image, DoG4, the area of the candidate MA, the perimeter of the candidate MA, the eccentricity of the candidate MA, the circularity of the candidate MA, the mean intensity of the candidate MA on shade corrected image and the ratio of the major axis length and minor length of the candidate MA. Fig. 4 shows an example of the MA pixels detected by the system in comparison with ground truth.

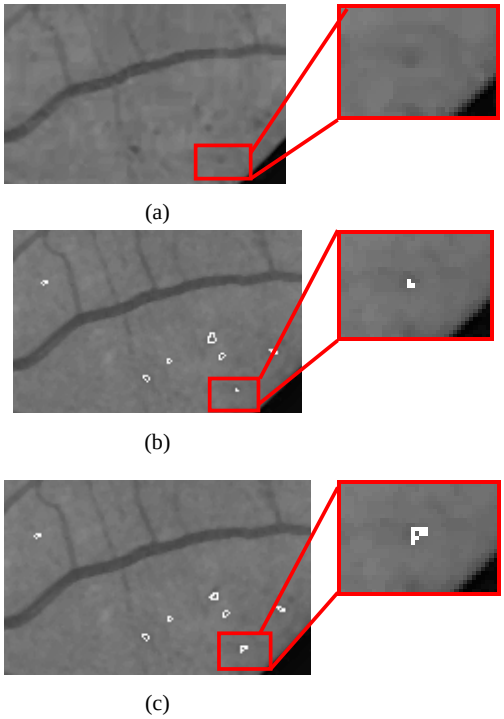

Fig. 4 Comparison of microaneurysm detection results (a) Original image (b) MA detected superimposed on original image (c) Ground truth image superimposed on original image

## ACKNOWLEDGMENT

This research is funded by the Burapha University, Chanthaburi Campus and National Research University Project of Thailand Office of Higher Education Commission (Thammasat University).

## REFERENCES

[1] S. Wild, G. Roglic, A. Green et al., "Global prevalence of diabetes: estimates for the year 2000 and projections for 2030," *Diabetes Care* 27, 2004, pp.1047-1053.
[2] P. Massin, A. Erginay, and A. Gaudric, "Retinopathie Diabetique", Elsevier, Editions scientifiques of medicales, Elsevier, SAS, Paris 2000.
[3] T. Spencer, J.A. Olson, K.C. McHardy et al., "An image-processingstrategy for the segmentation and quantification of microaneurysms in fluorescein angiograms of the ocular fundus," *Comp Biomed Res* 29, 1996, pp. 284–302.
[4] M.J. Cree, J.A. Olson, K.C. McHardy et al., "A fully automated comparative microaneurysm digital detection system," *Eye* 11, 1997, pp. 622–628.
[5] A. Frame, P. Undrill, M. Cree et al., "A comparison of computer based classification methods applied to the detection of microaneurysms in ophthalmic fluorescein angiograms," *Comput. Biol. Med.* 28, 1998, pp. 225–238.
[6] T. Walter, P. Massin, A. Erginay et al., "Automatic detection of microaneurysms in color fundus images," *Medical Image Analysis* 11(6), 2007, pp.555-566.
[7] C. Sinthanayothin, J.F. Boyce, T.H Williamson, T.H. et al., "Automated Detection of Diabetic Retinopathy on Digital Fundus Image," *Diabetic Medicine* 19(2), 2002, pp. 105–112, 2002.
[8] D. Usher, M. Dumskyj, M. Himaga et al., "Automated Detection of Diabetic Retinopathy in Digital Retinal Images: A Tool for Diabetic Retinopathy Screening," *Diabetic Medicine* 21(1), 2004, pp. 84–90.
[9] B. Dupas, T. Walter, A. Erginay et al., "Evaluation of automated fundus photograph analysis algorithms for detecting microaneurysms, haemorrhages and exudates, and of a computer-assisted diagnostic system for grading diabetic retinopathy," *Diabetes & Metabolism* 36(3), 2010, pp. 213-220.
[10] M. Niemeijer, B. van Ginneken, J. Staal et al., "Automatic detection of red lesions in digital color fundus photographs," *IEEE Trans Med Imaging* 24(5), 2005, pp.584-592.
[11] G. Gardner, D. Keating, T.H. Williamson et al., " Automatic detection of diabetic retinopathy using an artificial neural network: a screening tool," *Br J Ophthalmol* 80, 1996, pp.940–944.
[12] B. Zhang, X. Wu, J. You et al., "Detection of microaneurysms using multi-scale correlation coefficients," *Pattern Recognition* 43(6), 2010, pp. 2237-2248.
[13] A.Sopharak, B. Uyyanonvara, and S. Barman, Automatic Microaneurysm Detection from Non-dilated Diabetic Retinopathy Retinal Images Using Mathematical Morphological Methods. *IAENG International Journal of Computer Science* 38(3) (2011), 295-301.
[14] A. Sopharak, B. Uyyanonvara, S. Barman et al., "Automatic detection of diabetic retinopathy exudates from non-dilated retinal images using mathematical morphology methods," *Computer Medical Imaging and Graphics* 32(8), 2008, pp. 720-727.
[15] R.S. Kenneth, C.R. John, J. Matthew et al. (2006, June 15). Difference of Gaussians Edge Enhancement [Online]. Available: http://micro.magnet.fsu.edu/primer/java/digitalimaging/processing/diffgaussians/index.html
[16] N. Friedman, D. Geiger, and M. Goldszmidt, "Bayesian network classifiers," *Machine Learning*. Vol. 29, pp.131-163, 1997.
[17] O.D. Richard, E.H. Peter, and G.S. David, *Pattern Classification 2nd edition*, A Wiley-Interscience Publication, 2000, pp. 20-83.
[18] X.Y. Wang, J. Garibaldi, and T. Ozen, "Application of The Fuzzy C-Means clustering Method on the Analysis of non Pre-processed FTIR Data for Cancer Diagnosis," *Internat. Conf. on Australian and New Zealand Intelligent Information Systems (ANZIIS)*, pp. 233-238, 2003.